.

Photon noise from chaotic and coherent millimeter-wave sources measured with horn-coupled, aluminum lumped-element kinetic inductance detectors

D. Flanigan, , H. McCarrick, G. Jones, B. R. Johnson, M. H. Abitbol, P. Ade, D. Araujo, K. Bradford, R. Cantor, G. Che, P. Day, S. Doyle, C. B. Kjellstrand, H. Leduc, M. Limon, V. Luu, P. Mauskopf, A. Miller, T. Mroczkowski, C. Tucker, and J. Zmuidzinas

---

Articles you may be interested in

Horn-coupled, commercially-fabricated aluminum lumped-element kinetic inductance detectors for millimeter wavelengths
Review of Scientific Instruments **85**, 123117 (2014); 10.1063/1.4903855

High quality factor platinum silicide microwave kinetic inductance detectors
Applied Physics Letters **109**, 151102 (2016); 10.1063/1.4964665

Full characterisation of a background limited antenna coupled KID over an octave of bandwidth for THz radiation
Applied Physics Letters **110**, 233503 (2017); 10.1063/1.4985060

Broadband parametric amplifiers based on nonlinear kinetic inductance artificial transmission lines
Applied Physics Letters **110**, 152601 (2017); 10.1063/1.4980102

Photon noise from chaotic and coherent millimeter-wave sources measured with horn-coupled, aluminum lumped-element kinetic inductance detectors

D. Flanigan,[1,a)] H. McCarrick,[1] G. Jones,[1] B. R. Johnson,[1] M. H. Abitbol,[1] P. Ade,[2]
D. Araujo,[1] K. Bradford,[3] R. Cantor,[4] G. Che,[5] P. Day,[6] S. Doyle,[2] C. B. Kjellstrand,[1]
H. Leduc,[6] M. Limon,[1] V. Luu,[1] P. Mauskopf,[2,3,5] A. Miller,[1] T. Mroczkowski,[7] C. Tucker,[2]
and J. Zmuidzinas[6,8]

[1]*Department of Physics, Columbia University, New York, New York 10027, USA*
[2]*School of Physics and Astronomy, Cardiff University, Cardiff, Wales CF24 3AA, United Kingdom*
[3]*School of Earth and Space Exploration, Arizona State University, Tempe, Arizona 85287, USA*
[4]*STAR Cryoelectronics, Santa Fe, New Mexico 87508, USA*
[5]*Department of Physics, Arizona State University, Tempe, Arizona 85287, USA*
[6]*Jet Propulsion Laboratory, Pasadena, California 91109, USA*
[7]*Naval Research Laboratory, Washington, DC 20375, USA*
[8]*Division of Physics, Mathematics, and Astronomy, California Institute of Technology, Pasadena, California 91125, USA*

We report photon-noise limited performance of horn-coupled, aluminum lumped-element kinetic inductance detectors at millimeter wavelengths. The detectors are illuminated by a millimeter-wave source that uses an active multiplier chain to produce radiation between 140 and 160 GHz. We feed the multiplier with either amplified broadband noise or a continuous-wave tone from a microwave signal generator. We demonstrate that the detector response over a 40 dB range of source power is well-described by a simple model that considers the number of quasiparticles. The detector noise-equivalent power (NEP) is dominated by photon noise when the absorbed power is greater than approximately 1 pW, which corresponds to NEP $\approx 2 \times 10^{-17}$ W Hz$^{-1/2}$, referenced to absorbed power. At higher source power levels, we observe the relationships between noise and power expected from the photon statistics of the source signal: NEP $\propto P$ for broadband (chaotic) illumination and NEP $\propto P^{1/2}$ for continuous-wave (coherent) illumination. © *2016 Author(s). All article content, except where otherwise noted, is licensed under a Creative Commons Attribution 3.0 Unported License.* [http://dx.doi.org/10.1063/1.4942804]

A kinetic inductance detector[1] (KID) is a thin-film superconducting resonator designed to detect photons that break Cooper pairs. This detector technology is being developed for a range of applications across the electromagnetic spectrum. Our devices are being developed for cosmic microwave background (CMB) studies.

The randomness of photon arrivals sets the fundamental sensitivity limit for radiation detection. In recent years, several groups have used spectrally filtered thermal sources to perform laboratory measurements of both aluminum and titanium nitride KIDs that demonstrate sensitivity limited by photon noise.[2–6] Here, we use an electronic source to demonstrate photon-noise limited performance of horn-coupled, aluminum lumped-element kinetic inductance detectors[7] (LEKIDs) sensitive to a 40 GHz spectral band centered on 150 GHz.

The array of devices used in this study was fabricated by patterning a 20 nm aluminum film on a high-resistivity crystalline silicon substrate, with twenty detectors per array. Each resonator comprises lithographed structures that behave electrically as lumped elements, namely, an interdigitated capacitor and an inductive meander that is also the photon absorber. Schematics of a detector and the horn coupling scheme are shown in Figure 1. These devices were fabricated at STAR Cryoelectronics using the same lithographic mask used to

pattern the devices described in a previous study.[8] The same processing steps were used in this study except that the silicon wafer was immersed in hydrofluoric acid prior to aluminum deposition in order to clean and hydrogen-terminate the silicon surface to reduce oxide formation. We measure a superconducting transition temperature $T_c = 1.39$ K. The resonance frequencies are 95 MHz $< f_r <$ 195 MHz. Under the lowest loading conditions, the internal quality factors are $Q_i \approx 5 \times 10^5$. The coupling quality factors are $Q_c \approx 5 \times 10^4$. The volume of each inductive meander is 1870 μm^3, assuming nominal film thickness. The detector bath temperature is 120 ± 1 mK, obtained in a cryostat using an adiabatic demagnetization refrigerator backed by a helium pulse tube cooler. Detector readout is performed with a homodyne system using a cryogenic SiGe low-noise amplifier and open-source digital signal-processing hardware.[8,9] All the data shown are from a single representative detector with $f_r = 164$ MHz and were taken at a constant readout tone power of approximately -100 dBm on the feedline. The package that contains the detector chip is machined from QC-10, which is an aluminum alloy known to superconduct at the bath temperature used here.

Figure 1(a) is a schematic of the millimeter-wave source, located outside the cryostat. Within the source, the output of a 12× active multiplier chain passes through two variable waveguide attenuators that allow the output power to be controlled over a range of more than 50 dB. The

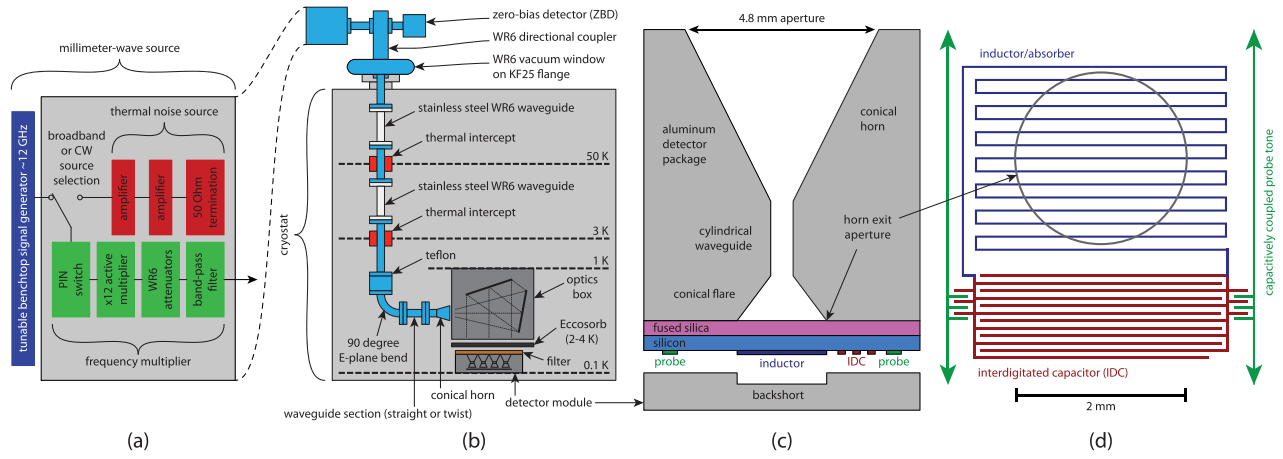a)Electronic mail: daniel.flanigan@columbia.edu

FIG. 1. Experiment schematics. (a) The millimeter-wave source components. (b) The source and cryogenic setup. (c) A cross-section of an array element. The inner conical flare and fused silica layer are designed for impedance matching. (d) The lumped circuit elements of one LEKID. Parts of this figure are reproduced with permission from H. McCarrick *et al.*, Rev. Sci. Instrum. **85**, 123117 (2014). Copyright 2014 AIP Publishing LLC.

primary components of the source are listed in the supplementary material.[10]

The output spectrum is controlled by a band-pass filter with a sharp roll-off outside its passband of 140 to 160 GHz. Within this passband, the source can produce radiation in two modes. In *broadband* mode, amplified noise is multiplied into a broadband chaotic signal. In *continuous-wave* mode, a multiplied tone from a signal generator approximates a monochromatic coherent signal. We have measured the source output in both modes using a Fourier transform spectrometer; these measurements show that in broadband mode the power is constant within a factor of two across the output band, and in continuous-wave mode, it appears monochromatic with negligible higher harmonics.

Figure 1(b) shows the signal path from the source through the cryostat to the detectors. The source output is split using a waveguide directional coupler that sends 99% of the power into a calibrated, isolator-coupled zero-bias diode power detector (ZBD), the voltage output of which is recorded using a lock-in amplifier. The remaining 1% of the power travels through a vacuum window and into the cryostat through WR6 waveguide. A piece of Teflon at 4 K inserted into the waveguide absorbs room-temperature thermal radiation. Two mirrors transform the output of a conical horn into a collimated beam. A 6.4 mm thick slab of microwave absorber (Eccosorb MF-110), regulated at 2 K during these measurements, attenuates incoming signals and provides a stable background load. A metal-mesh filter at the detector apertures defines the upper edge of the detector band at 170 GHz. The lower edge of the band at 130 GHz is defined by the cutoff frequency of a 1.35 mm diameter circular waveguide in the detector package. We note that the source output is within the single-mode bandwidth of both WR6 waveguide and the circular waveguide. The radiation from the source incident on the detector horns is linearly polarized, and the electric field is aligned with the long elements of the inductive meanders in the detectors.

Figure 2 shows the main results of this work. All power values in this figure refer to the power from the source absorbed by the detector: $P_A = \eta_S P_S$, where P_S is measured by the ZBD. Before calibration, the efficiency η_S is known

only approximately from measurements and simulations of the components between the source and the detector. We accurately determine η_S, and thus the absorbed source power, by measuring the relationship between emitted source power and detector noise. This calibration relies on the assumption that all components between the source output and detector are linear: We have linearized the ZBD response at the higher power levels, all other components are passive, and we assume that filter heating is negligible. To perform the calibration we use measurements of the noise-equivalent power (NEP), defined as the standard error of the mean in the inferred optical power at a given point in the optical system after 0.5 s of integration.[11,12] We calculate the NEP using measurements of the detector noise and responsivity.

At each source power level, to determine the resonance frequency and the quality factors, we sweep the readout tone generator frequency f_g across a resonance and fit a resonator model to the forward scattering parameter $S_{21}(f_g)$ data.[8] Figure 2(c) shows the detector response to source power in both broadband and continuous-wave modes. At low source power in both modes, the fractional frequency shift $x(P_A) = f_r(0)/f_r(P_A) - 1$ is approximately linear in power, while at high power $x \propto P_A^{1/2}$. This behavior is described by a model in which the fractional frequency shift is proportional to the number of quasiparticles

$$N_{qp} = N_*[(1 + 2\tau_{max}(\Gamma_0 + \Gamma_S)/N_*)^{1/2} - 1]. \quad (1)$$

Here, $\Gamma_S \propto P_A$ is the rate of quasiparticle generation due to absorbed source photons, Γ_0 is the constant generation rate due to other effects (such as absorption of ambient photons and thermal phonons), and N_* and τ_{max} are material-dependent constants that describe the observed saturation of the quasiparticle relaxation time at low quasiparticle number:[13] $\tau_{qp} \approx \tau_{max}/(1 + N_{qp}/N_*)$. (This saturation is not experimentally accessible here.) We calculate the responsivity dx/dP_S at each source power level with a finite-difference derivative that uses the fractional frequency response at adjacent power levels.

To measure detector noise, we record time-ordered data $S_{21}(f_g = f_r)$. Using the resonator model from the fit to the
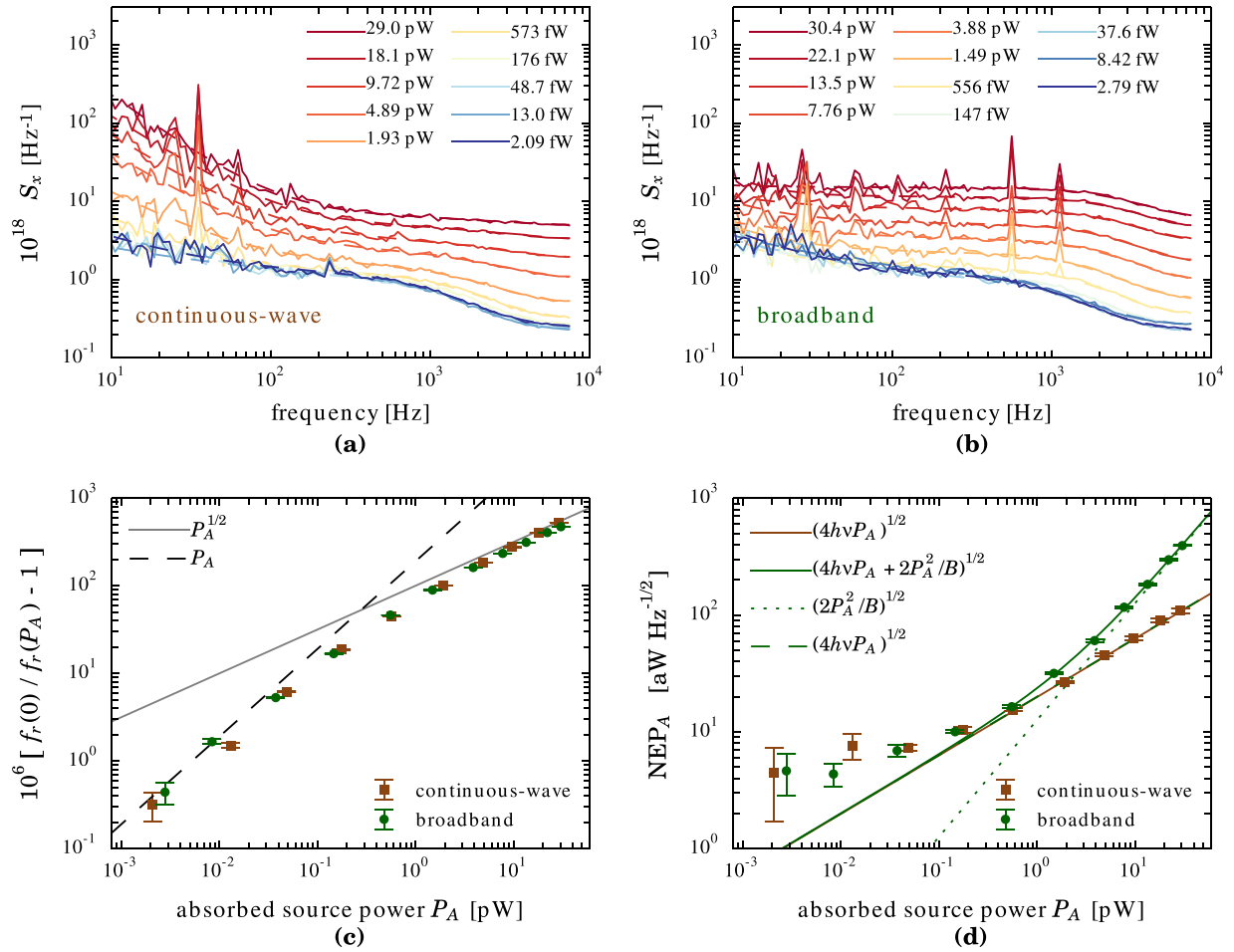
FIG. 2. Primary results of the experiment. (a) Spectral density S_x of detector time-ordered data versus frequency under continuous-wave illumination with $\nu = 148$ GHz (solid lines), and the result of fitting the data to Equation (2) (dashed lines). At high power, the red noise component is dominated by fluctuations from the signal generator that feeds the multiplier; these fluctuations are correlated among detectors. (b) Spectral density under broadband illumination, and fits of Equation (2). The spikes above 400 Hz are pickup from a fan in the source. The red noise below 100 Hz at low source power in both modes is produced by vibrations from the pulse tube cooler that vanish when it is turned off. The detector white noise levels from the fits are used to calculate NEP values. (c) Fractional frequency response versus absorbed power in both source modes. The error bars are statistical errors from the resonator fits. We use the finite-difference derivative of these response data to calculate the NEP. The dashed black line and solid gray line are guides that show how the response scales at both low and high absorbed power. (d) Noise-equivalent power versus absorbed power in both source modes. All data points and lines are referenced to absorbed power. The error bars are propagated statistical errors from the finite difference derivative and the detector noise fits. The solid green line is the sum of the quadratic and linear terms in the fit of Equation (6) to the broadband NEP^2 data. The dotted green line is the quadratic term, which is the photon wave noise contribution. The dashed green line is the linear term, which contains equal contributions from photon shot noise and quasiparticle recombination noise. The broadband frequency used is $\nu = 150$ GHz, near the band center. The solid brown line (nearly coincident with dashed green) is the linear term in the fit of Equation (6) to the continuous-wave NEP^2 data, in which the quadratic term is omitted.

frequency sweep, we convert these data into units of fractional frequency shift x and then calculate the single-sided spectral density $S_x(f)$. Figures 2(a) and 2(b) show the measured noise spectra and fits to the following model:[10]

$$S_x(f) = W^2 \frac{1 + (f_k/f)^\alpha}{1 + (f/f_c)^2} + A^2, \qquad (2)$$

where the free parameters are the detector white noise W^2, the red noise knee frequency f_k, the spectral index α, the cut-off frequency f_c, and the amplifier noise A^2. This model treats the detector noise as the sum of a white noise process with spectral density W^2 and a red noise process with spectral density $R^2 = W^2(f_k/f)^\alpha$, both rolled off at f_c.

The detector audio bandwidth of about 1 kHz corresponds to a limiting time constant $\tau = (2\pi f_c)^{-1}$ that is approximately equal to both the resonator ring-down time $\tau_r = Q/\pi f_r$ and the expected quasiparticle relaxation time τ_{qp} for aluminum. Both of these time constants are expected to

decrease as the absorbed optical power increases, as observed in the data.

To model the detector noise, we first consider noise sources independent of the quasiparticle system. White noise due to the cryogenic amplifier dominates at frequencies well above the detector bandwidth, and we account for it in the noise spectra model. Two-level systems (TLS) in amorphous dielectric surface layers located near the resonator produce fluctuations in the local dielectric constant and thus in f_r.[14] In a separate experiment, described in the supplementary material,[10] we determined that TLS noise is negligible at the readout power level (-100 dBm) used in the measurements presented here and thus do not include it in the noise model. The chosen readout power level is high enough to suppress TLS noise but is not so high that nonlinear effects due to resonator bifurcation become significant.

The remaining noise sources involve fluctuations in the quasiparticle system: Generation by optical photons,

readout photons, and thermal phonons, as well as quasiparticle recombination, e.g., via phonon emission. All of these sources are expected to produce white noise that rolls off at the frequency corresponding to the larger of τ_r and τ_{qp}.[13] We expect readout generation to be negligible at high source power and treat it as constant. (Where present, the photon wave noise introduces correlations between photon arrival times. This noise has a bandwidth equal to the 20 GHz bandwidth of the absorbed broadband radiation, so it is also expected to appear white in the detector audio band.[15])

The NEP model includes theoretical expectations for photon noise and quasiparticle recombination noise. We denote by n the mean photon occupancy of a single spatial/polarization mode of the electromagnetic field with frequency ν. For example, for a thermal source at temperature T, the occupancy is $n = [\exp(h\nu/k_B T) - 1]^{-1}$, where h is Planck's constant and k_B is Boltzmann's constant. If we assume that the radiation occupies an effective optical bandwidth $B \ll \nu$ sufficiently narrow that quantities such as occupancy and absorption efficiency can be treated as constant, then the power from this mode that is absorbed by a detector with absorption efficiency η is $P_A = \eta n B h\nu$. If the source is thermal, then the contribution of photon noise to the NEP is given by[12]

$$\mathrm{NEP}_{A,\gamma}^2 = 2\eta n(1 + \eta n)B(h\nu)^2 = 2h\nu P_A + 2P_A^2/B, \quad (3)$$

which is referenced to absorbed power. We refer, respectively, to these two terms as shot noise and wave noise, following Hanbury Brown and Twiss.[16] If the source is monochromatic with perfect temporal coherence, then only the shot noise term is present regardless of the occupancy: this behavior represents a key difference between a quantum coherent state and a quantum-statistical thermal state of the field.[17,18] For a thermal source, if $\eta n \ll 1$, the shot noise dominates, which is typical in optical astronomy; if $\eta n \gg 1$, the wave noise dominates, which is typical in radio astronomy.

We measure power at the output of the source and detector NEP referenced to the same point. Referencing the photon NEP to the source output gives

$$\mathrm{NEP}_{S,\gamma}^2 = \mathrm{NEP}_{A,\gamma}^2/\eta_S^2 = 2h\nu P_S/\eta_S + 2P_S^2/B. \quad (4)$$

The presence of the efficiency η_S in the linear term of this equation enables extraction of the absorbed source power.

Previous studies that calculated the absorption efficiency of a KID by measuring the scaling of photon shot noise with optical power have used superconducting films with transition temperatures similar to the film used here but larger photon energies.[2,3,5,6] Here, the photons have energies $h\nu \gtrsim 2\Delta$, where Δ is the superconducting energy gap, so each photon excites only two quasiparticles close to the gap; in this limit the quasiparticle recombination noise is significant. The recombination noise contribution to NEP_A is[10]

$$\mathrm{NEP}_{A,R}^2 = 4\Delta P_A/\eta_{pb}, \quad (5)$$

where η_{pb} is the pair-breaking efficiency. For photon energies $2\Delta < h\nu < 4\Delta$, a recent measurement[19] found $\eta_{pb} \approx 2\Delta/h\nu$, in agreement with theory.[20] Using this value, the

recombination NEP equals the shot noise term in the photon NEP. This is expected based on the symmetry between uncorrelated pair-breaking events and uncorrelated pair-recombination events. Finally, we introduce a small constant term NEP_0 to account for noise sources independent of source power, such as TLS noise and quasiparticle generation-recombination noise from thermal phonons, readout photons, and ambient photons.

To calculate the detector NEP_A, which is shown in Figure 2(d), we use the measured fractional frequency shift x (unitless), the measured fractional frequency noise power S_x (1/Hz), and the source power P_S (watts) as measured with a calibrated ZBD mounted on the directional coupler outside the cryostat (see Figure 1). The source power absorbed by the detector is related to P_S by $P_A = \eta_S P_S$, where η_S is an overall system efficiency from the source output to the detector that includes the transmission through the directional coupler, the attenuation of the stainless steel waveguide, the geometrical dilution due to the internal optics, the loss in the Eccosorb, and the detector absorption efficiency. To compute the responsivity to changes in the source power, we plot x versus P_S and calculate the slope of this curve dx/dP_S at each P_S using a finite difference algorithm. We use this responsivity to convert the fractional frequency noise measurements (S_x) to NEP_S. Note that for NEP_S, we use only the white noise component, W, obtained by fitting Equation (2) to each S_x measurement. Thus, $\mathrm{NEP}_S = W/(dx/dP_S)$. To convert P_S to P_A, we need to determine η_S. The complete theoretical model for NEP_S is

$$
\begin{aligned}
\mathrm{NEP}_S^2 &= (\mathrm{NEP}_{A,0}^2 + \mathrm{NEP}_{A,R}^2 + \mathrm{NEP}_{A,\gamma}^2)/\eta_S^2 \\
&= \mathrm{NEP}_{A,0}^2/\eta_S^2 + [2(2h\nu P_A) + 2P_A^2/B]/\eta_S^2 \\
&= \mathrm{NEP}_{S,0}^2 + 4h\nu P_S/\eta_S + 2P_S^2/B, \quad (6)
\end{aligned}
$$

which is the sum of the aforementioned noise contributions. The right-hand side of this equation is quadratic in P_S with unknown quantities $\mathrm{NEP}_{S,0}$, η_S, and effective optical bandwidth B. The limiting $\mathrm{NEP}_{S,0}$ is discussed below. We fit Equation (6) to the broadband data using center frequency $\nu = 150$ GHz and obtain $\eta_S = 8.50 \times 10^{-7}(1\pm 0.09)$ and $B = 13$ GHz. The quadratic term is not expected to be present for coherent illumination because the source should produce only shot noise, so we fit Equation (6) to the continuous-wave data omitting the third term. Here, $\nu = 148$ GHz and we obtain $\eta_S = 1.12 \times 10^{-6}(1\pm 0.04)$. As a final step, we convert P_S to P_A using the η_S values from the model fitting and produce Figures 2(c) and 2(d). Note that because the broadband source involves contributions from the full source output bandwidth, it is not surprising that the measured η_S values differ between the continuous-wave and broadband modes by more than the statistical error bars.

Figure 2(d) shows that photon noise dominates under broadband illumination when $P_A \gtrsim 1$ pW, which corresponds to $\mathrm{NEP}_A \approx 2 \times 10^{-17}$ W Hz$^{-1/2}$. At high power in each source mode, we observe the expected relationship between noise and power: in broadband mode $\mathrm{NEP} \propto P$ because the quadratic wave noise term dominates, while in continuous-wave mode $\mathrm{NEP} \propto P^{1/2}$ because the quadratic term is not present. This behavior is a clear signature of photon noise.

Note that the NEP_A values reported have the amplifier noise contribution subtracted because the white noise parameter W^2 in Equation (2) describes the noise power above the amplifier noise A^2. Here, subtracting the amplifier noise yields an accurate estimate of the detector performance because, alternatively, the amplifier noise can be suppressed to a negligible level by increasing the readout power. We verified both approaches yield the same NEP_A versus P_A result but chose to report the amplifier-noise-subtracted results.

At low absorbed source power levels in both modes, where $P_A < 0.1\,pW$, NEP_A levels off to NEP_0. The values of NEP_0 extracted from both of the aforementioned fits are approximately 5–$6 \times 10^{-18}\,W\,Hz^{-1/2}$. To explain this leveling-off effect, we model the background loading as emission from a black body at $2\,K$, which is the temperature of the Eccosorb in front of the feed horn apertures. Assuming center frequency $\nu = 150\,GHz$, optical efficiency $\eta_I = 0.7$ (obtained from electromagnetic simulations), and detector bandwidth $B_{full} = 40\,GHz$, then the radiative loading from the Eccosorb is $P_A = \eta_I n(\nu, 2\,K) h\nu B_{full} = 0.08\,pW$. This loading level is close to the observed knee in the curves in Figure 2(d). Adding an equal recombination noise contribution to the corresponding photon NEP gives $NEP_A = (2 \cdot 2h\nu P_A)^{1/2} = 5.6 \times 10^{-18}\,W\,Hz^{-1/2}$, which is close to the observed NEP_0 value. Therefore, the observed limiting NEP_A is consistent with this expected background loading model.

Analysis of data from twelve detectors yielded similar results to those shown in Figure 2(d), with the photon noise starting to dominate between 0.5 and 1 pW. We conclude that these detectors become limited by photon noise at absorbed power levels lower than the background power levels already measured by ground-based CMB polarimeters.

[1]P. K. Day, H. G. LeDuc, B. A. Mazin, A. Vayonakis, and J. Zmuidzinas, Nature **425**, 817 (2003).

[2]S. J. C. Yates, J. J. A. Baselmans, A. Endo, R. M. J. Janssen, L. Ferrari, P. Diener, and A. M. Baryshev, Appl. Phys. Lett. **99**, 073505 (2011).

[3]R. M. J. Janssen, J. J. A. Baselmans, A. Endo, L. Ferrari, S. J. C. Yates, A. M. Baryshev, and T. M. Klapwijk, Appl. Phys. Lett. **103**, 203503 (2013).

[4]P. D. Mauskopf, S. Doyle, P. Barry, S. Rowe, A. Bidead, P. A. R. Ade, C. Tucker, E. Castillo, A. Monfardini, J. Goupy, and M. Calvo, J. Low Temp. Phys. **176**, 545 (2014).

[5]P. de Visser, J. J. A. Baselmans, J. Bueno, N. Llombart, and T. M. Klapwijk, Nat. Commun. **5**, 3130 (2014).

[6]J. Hubmayr, J. Beall, D. Becker, H.-M. Cho, M. J. Devlin, B. Dober, C. Groppi, G. C. Hilton, K. D. Irwin, D. Li *et al.*, Appl. Phys. Lett. **106**, 073505 (2015).

[7]S. Doyle, P. Mauskopf, J. Zhang, A. Monfardini, L. J. Swenson, J. J. A. Baselmans, S. J. C. Yates, and M. Roesch, Proc. SPIE **7741**, 77410M (2010).

[8]H. McCarrick, D. Flanigan, G. Jones, B. R. Johnson, P. A. R. Ade, D. Araujo, K. Bradford, R. Cantor, G. Che, P. Day *et al.*, Rev. Sci. Instrum. **85**, 123117 (2014).

[9]See http://www.github.com/ColumbiaCMB for the software used to read out the detectors and analyze the data.

[10]See supplementary material at http://dx.doi.org/10.1063/1.4942804 for a list of the millimeter-wave source components, analysis of TLS noise and recombination noise contributions, and detail of the spectral density fitting process.

[11]P. L. Richards, J. Appl. Phys. **76**, 1 (1994).

[12]J. Zmuidzinas, Appl. Opt. **42**, 4989 (2003).

[13]J. Zmuidzinas, Annu. Rev. Condens. Matter Phys. **3**, 169 (2012).

[14]J. Gao, M. Daal, J. M. Martinis, A. Vayonakis, J. Zmuidzinas, B. Sadoulet, B. A. Mazin, P. K. Day, and H. G. LeDuc, Appl. Phys. Lett. **92**, 212504 (2008).

[15]J. Zmuidzinas, ApJ **813**, 17 (2015).

[16]R. Hanbury Brown and R. Q. Twiss, Proc. R. Soc. A **242**, 300 (1957).

[17]R. Loudon, *The Quantum Theory of Light*, 3rd ed. (Oxford University Press, Oxford, 2002).

[18]R. J. Glauber, see http://www.nobelprize.org, "Nobel Lecture: One Hundred Years of Light Quanta."

[19]P. de Visser, S. J. C. Yates, T. Guruswamy, D. J. Goldie, S. Withington, A. Neto, N. Llombart, A. M. Baryshev, T. M. Klapwijk, and J. J. A. Baselmans, Appl. Phys. Lett. **106**, 252602 (2015).

[20]T. Guruswamy, D. J. Goldie, and S. Withington, Supercond. Sci. Technol. **27**, 055012 (2014).